

Published in final edited form as:

*Cell Cycle*. 2008 May 15; 7(10): 1490–1495.

## Oxidative stress induces cell cycle-dependent Mre11 recruitment, ATM and Chk2 activation and histone H2AX phosphorylation

Hong Zhao<sup>1</sup>, Frank Traganos<sup>1</sup>, Anthony P. Albino<sup>2</sup>, and Zbigniew Darzynkiewicz<sup>1,\*</sup>

<sup>1</sup>*Brander Cancer Research Institute and Department of Pathology; New York Medical College; Valhalla, New York USA*

<sup>2</sup>*Vector Research Ltd.; New York, New York USA*

### Abstract

DNA damage response recruits complex molecular machinery involved in DNA repair, arrest of cell cycle progression, and potentially in activation of apoptotic pathway. Among the first responders is the Mre11- (MRN) complex of proteins (Mre11, Rad50, Nbs1), essential for activation of ATM; the latter activates checkpoint kinase 2 (Chk2) and phosphorylates histone H2AX. In the present study the recruitment of Mre11 and phosphorylation of ATM, Chk2 and H2AX ( $\gamma$ H2AX) detected immunocytochemically were measured by laser scanning cytometry to assess kinetics of these events in A549 cells treated with H<sub>2</sub>O<sub>2</sub>. Recruitment of Mre11 was rapid, peaked at 10 min of exposure to the oxidant, and was of similar extent in all phases of the cell cycle. ATM and Chk2 activation as well as H2AX phosphorylation reached maximum levels after 30 min of treatment with H<sub>2</sub>O<sub>2</sub>; the extent of phosphorylation of each was most prominent in S-, less in G<sub>1</sub>-, and the least in G<sub>2</sub>M- phase cells. A strong correlation between activation of ATM and Chk2, measured in the same cells, was seen in all phases of the cycle. In untreated cells activated Chk2 and Mre11 were distinctly present in centrosomes while in interphase cells they had characteristic punctate nuclear localization. The punctate expression of activated Chk2 both in untreated and H<sub>2</sub>O<sub>2</sub> treated cells was accentuated when measured as maximal pixel rather than integrated value of immunofluorescence (IF) per nucleus, and was most pronounced in G<sub>1</sub> cells, likely reflecting the function of Chk2 in activating Cdc25A. Subpopulations of G<sub>1</sub> and G<sub>2</sub>M cells with strong maximal pixel of Chk2-Thr68<sup>P</sup> IF in association with centrosomes were present in untreated cultures. Cytometric multiparameter assessment of the DNA damage response utilizing quantitative image analysis that allows one to measure inhomogeneity of fluorochrome distribution (e.g., maximal pixel) offers unique advantage in studies of the response of different cell constituents in relation to cell cycle position.

### Keywords

reactive oxygen species; hydrogen peroxide; DNA damage response; apoptosis; checkpoint; centrosome; mitosis

### Introduction

Oxidative DNA damage, considered one of the major causes of cell aging and suspected to precondition to cancer, is being caused by reactive oxygen species (ROS) either generated during aerobic respiration,<sup>1-9</sup> or originating from exogenous sources such as environmental pollutants,<sup>10</sup> macrophage oxidative burst,<sup>11-13</sup> or even iatrogenic factors.<sup>14</sup> Oxidation of all

\*Correspondence to: Zbigniew Darzynkiewicz; Brander Cancer Research Institute at NYMC; Department of Pathology; BSB 438; Valhalla, New York 10595 USA; Tel.: 914.594.3780; Fax: 914.594.3790; Email: darzynk@nyc.edu

four DNA bases [with a predominance of guanine adducts such as 8-oxo-7,8-dihydro-2'-deoxyguanosine (oxo8dG)], base ring fragmentation, sugar modification, covalent crosslinking of DNA and protein, and induction of DNA strand breaks, all may occur as a result of oxidative DNA damage.<sup>2,15,16</sup> Some of these lesions are converted, predominantly during DNA replication, to DNA double-strand breaks (DSBs).<sup>7</sup> Repair of some DSBs can be error prone resulting in deletion of base pairs and other defects that can result in translocations and chromosomal instability.<sup>3,4,17,18</sup> Cumulative alterations of the molecular structure of DNA is thought to play important roles in the genesis of organismic aging, cellular senescence, and predisposition to cancer.<sup>1-6,19-21</sup> We have recently reviewed this topic and in particular addressed the issue of constitutive DNA damage caused by metabolically generated endogenous oxidants and its detection by cytometry.<sup>8,9,22-24</sup>

In our previous studies<sup>8,9,22-26</sup> we monitored DNA damage indirectly, by immunocytochemical assessment of histone H2AX phosphorylation<sup>27</sup> and activation of the *Ataxia telangiectasia* mutated protein kinase (ATM).<sup>28,29</sup> These molecular targets have already been extensively used in conjunction with cytometry, to assess the extent of DNA damage induced by exogenous agents and to correlate damage with the cell cycle phase and induction of apoptosis.<sup>22-26,30-38</sup> However, DNA damage also activates checkpoint pathways to arrest progression through the cell cycle until DNA integrity is restored by the repair process.<sup>39-42</sup> Activation of checkpoint kinase 2 (Chk2) plays a major role in arresting the cell cycle progression machinery in response to DNA damage.<sup>40-42</sup> In most instances activation of Chk2 is mediated by ATM which directly phosphorylates Thr68 of this kinase inducing its dimerization which is followed by intermolecular phosphorylation on Thr383, Thr387 and Ser516, dissociation of the dimers and formation of enzymatically active monomers.<sup>39-42</sup> The major physiological substrates of Chk2 are the phosphatases Cdc25C and Cdc25A. Phosphorylation of Cdc25C and Cdc25A by Chk2 prevents their translocation and the dephosphorylation of cyclin dependent kinases (CDKs), an event otherwise essential for G<sub>2</sub> to M and G<sub>1</sub> to S transitions, respectively.<sup>43,44</sup> Proteasomal degradation of Cdc25 phosphatases is also accelerated upon their phosphorylation.<sup>45</sup> Thus, as a consequence of Chk2 activation the cells can arrest at the G<sub>2</sub> to M and/or G<sub>1</sub> to S transition.<sup>46</sup> It should also be noted that the MRN complex of proteins consisting of Mre11-Rad50-NBS1 is essential for ATM activation, as it recognizes DNA damage, recruits ATM to the site of damage and targets ATM to initiate phosphorylation of the respective substrates.<sup>47-51</sup>

In the present study we compared the kinetics of ATM and Chk2 activation and H2AX phosphorylation in response to oxidative DNA damage in human lung adenocarcinoma A549 cells and correlated these data to the expression of the Mre11 protein. The results demonstrate a rapid DNA damage response to oxidative damage that is reflected by a nearly concurrent increase in expression of Mre11, activation of ATM and Chk2 and phosphorylation of H2AX, peaking at 10–30 min after exposure of A549 cells to H<sub>2</sub>O<sub>2</sub>.

## Results

Figure 1 illustrates the effect of H<sub>2</sub>O<sub>2</sub> exposure on expression of Mre11 in the nuclei of A549 cells. The data show a distinct increase in Mre11 IF intensity that is observable by 10 min post-exposure to the oxidant. The intensity of Mre11 IF in a large majority of A549 cells treated for 10 min with H<sub>2</sub>O<sub>2</sub> was well above the background level of the untreated cells (skewed dashed line), representing the upper threshold of Mre11 IF for 97% of the untreated interphase cells. There was no evidence of a cell cycle phase specificity in response to H<sub>2</sub>O<sub>2</sub>, as the observed increase in Mre11 IF was similar for cells in G<sub>1</sub>, S and G<sub>2</sub>M. The pattern of response to H<sub>2</sub>O<sub>2</sub> was somewhat different when measured either as integrated or maximal pixel of Mre11 IF, the former reflecting total IF per nucleus the latter stressing the punctate (foci) distribution of this protein (Fig. 1). The intercellular variability was distinctly more apparent when Mre11

expression was measured as maximal pixel of IF rather than as the integrated IF value. The cells treated with H<sub>2</sub>O<sub>2</sub> for 2 h had lower expression of Mre11 than 10 min treated cells, but still above the level of untreated cells.

Exposure of A549 cells to H<sub>2</sub>O<sub>2</sub> also induced both ATM activation and H2AX phosphorylation (Fig. 2). While the cellular responses in terms of ATM activation and H2AX were quite similar in terms that maximally affected were S-phase cells, it differed considerably from the Mre11 response that showed no cell cycle phase specificity. In cultures treated with the oxidant for 10 or 30 min, essentially all S-phase cells had ATM-S1981<sup>P</sup> and  $\gamma$ H2AX IF values above the background level of the untreated cells representing the upper threshold of expression of these phospho-proteins for 97% of the interphase cells. Also, both the expression of ATM-S1981<sup>P</sup> and  $\gamma$ H2AX were maximal in cells treated with H<sub>2</sub>O<sub>2</sub> for 30 min, followed by a decrease that was apparent in cells treated with H<sub>2</sub>O<sub>2</sub> for 1–4 h. Analysis of DNA content frequency histograms show no significant changes in cell cycle distribution during the treatment with H<sub>2</sub>O<sub>2</sub> for 4 h with the exception of a minor accumulation of cells in very early S-phase (Fig. 2; arrow).

Activation of Chk2 in response to oxidative DNA damage is illustrated in Figure 3. The data show very early activation of this protein kinase, apparent 10 min after cells exposure to the oxidant, and declining after 30 min. Here again, as with ATM activation and H2AX phosphorylation, S phase cells were most affected. It should be stressed that significantly different cellular response pattern to DNA damage was observed when signal intensity was measured as either an integrated Chk2-Thr68<sup>P</sup> IF value (Fig. 3; top) or as maximal pixel values (bottom). In untreated (time 0) cultures the strong integrated Chk2-Thr68<sup>P</sup> IF was observed only in mitotic cells. However, when Chk2-Thr68<sup>P</sup> IF was expressed as a maximal pixel value it revealed the presence of G<sub>1</sub> and G<sub>2</sub>M cells with high maximal pixel values (Fig. 3, outlined by oval dashed boundaries). Analysis of the images revealed an association of Chk2-Thr68<sup>P</sup> IF with the centrosomes in these cells. The G<sub>1</sub> cells with high maximal pixel values for Chk2-Thr68<sup>P</sup> were predominantly very early (postmitotic) G<sub>1</sub> cells, which could be identified by LSC as cells with very small nuclear size that were in close proximity with each other as they would be just after cytokinesis (not shown). In support of this observation is the bivariate distribution pattern showing that the cells entering S-phase (late G<sub>1</sub> cells, in continuity with the S-cell cluster) had low Chk2-Thr68 maximal pixel IF values. Interestingly, while exposure to H<sub>2</sub>O<sub>2</sub> for 2 and 4 h led to a marked *decrease* in intensity of integral values of Chk2-Thr68<sup>P</sup> IF, a distinct subpopulation of cells with a G<sub>1</sub> DNA content and very strong maximal pixel IF become apparent and their fluorescence intensity was on *increase* (Fig. 3, delineated by rectangular dashed outlines and marked by triangular arrows). On the bivariate distributions these cells are clearly not continuous with the S-phase cell cluster.

A strong correlation was observed between activation of ATM and Chk2 when measured in the same cells. The data (Fig. 4) show cells responding to 10 min and 1 h treatment with H<sub>2</sub>O<sub>2</sub>. This correlation was apparent regardless of whether all cells, or only S-phase cells, were analyzed. An exception was the presence of relatively few (~3%) cells with activated Chk2 but with no apparent ATM activation, predominantly present in the untreated culture (Fig. 4, marked by arrows). The image analysis revealed that these were mitotic cells. In fact, these cells had activated ATM. However ATM-S1981<sup>P</sup> was in cytoplasm of mitotic cells and the fluorescence integration (contouring) based on DNA (DAPI fluorescence) excluded cytoplasmic fluorescence. Activated Chk2 on the other hand was present both in cytoplasm and in association with mitotic chromosomes.

The kinetics of response to H<sub>2</sub>O<sub>2</sub>-induced DNA damage measured by Mre11 recruitment, ATM and Chk2 activation and H2AX phosphorylation is presented in Figure 5. The increase in expression of Mre11 was rapid, peaking after a 10 min exposure to H<sub>2</sub>O<sub>2</sub> followed by a slow

decline. Activation of ATM and Chk2 was also rapid with the maximal level of their phosphorylation observed after 10–30 min of treatment with H<sub>2</sub>O<sub>2</sub>. Histone H2AX phosphorylation peaked after 30 min as well. Whereas the increase in expression of Mre11 was similar in extent for cells in all phases of the cell cycle, activation of ATM, Chk2 and H2AX phosphorylation was most pronounced for S-phase cells while G<sub>2</sub>M cells were least affected. The maximal increase was observed for H2AX phosphorylation, with the level of  $\gamma$ H2AX expression in S-phase cells after 30 min of treatment with H<sub>2</sub>O<sub>2</sub> being over 300% (>3.00 fold) above that of untreated cells in S phase. The maximum ATM phosphorylation observed was over 200% above the level of untreated cells. The increase in expression of Chk2-Thr68<sup>P</sup> and Mre11 was less pronounced reaching only 135% and 75%, respectively, over the level of the untreated cells.

The characteristic subcellular localization of Chk2-Thr68<sup>P</sup>, ATM-S1981<sup>P</sup> and Mre11 is presented in Figure 6. In mitotic cells activated Chk2 was distinctly present in centrosomes and also in the cytoplasm where it had a discrete punctate appearance. In interphase cells the Chk2-Thr68<sup>P</sup> IF was also punctate but was localized in the nuclei, and was more intense in cells exposed to H<sub>2</sub>O<sub>2</sub> than in the untreated cells. ATM was also strongly activated in mitotic cells and was present in their cytoplasm, whereas its localization in H<sub>2</sub>O<sub>2</sub> treated interphase cells was nuclear. IF of Mre11 was strong in untreated cells but was distinctly stronger in the H<sub>2</sub>O<sub>2</sub> treated ones where it was mostly limited to nuclei and also had a punctate appearance. Mre11 was also present in centrosomes of mitotic cells (Fig. 6).

## Discussion

The present data reveal the kinetics of the DNA damage response of A549 cells to the oxidant H<sub>2</sub>O<sub>2</sub>. This is the first report which describes an increase in expression of Mre11 measured by cytometry, in cells treated with a DNA damaging agent. The observed rise in Mre11 expression, although less extensive than that of phosphorylation of ATM, Chk2 or H2AX, was very rapid, peaking at 10 min. It is unclear whether this effect, detected immunocytochemically so early after administration of H<sub>2</sub>O<sub>2</sub>, reflects an increase in content of Mre11 protein due to its synthesis or increased accessibility of the epitope during formation of MRN complexes. The epitope of Mre11 detected by this Ab (31H4, rabbit) is a small peptide domain corresponding to Lys496 of human Mre11A.<sup>52</sup> Because the expression of Mre11 (as with ATM-S1981<sup>P</sup>, Chk2-Thr68<sup>P</sup> and H2AX) was measured within the cells nucleus (the integration contour was set up on DAPI fluorescence) the apparent increase in Mre11 expression may also be due to its migration from the cytoplasm to the nucleus. As the increase in Mre11 expression was modest (~75% above the level of untreated cells) the nuclear translocation of even minor amounts may account for such an effect. Regardless of the mechanism, it is clear from our data that signaling through MRN translocation that involves Mre11 recruitment, considered the earliest response to DNA damage prior even to ATM activation,<sup>47-50</sup> is detectable by cytometry.

Activation of Chk2 serves primarily to arrest cell cycle progression and because of functional redundancy in its ability to phosphorylate both, Cdc25A and Cdc25C, both the G<sub>1</sub> to S and G<sub>2</sub> to M transitions, may be halted.<sup>43,46</sup> We show here that Chk2 activation was rapid, concurrent to- and strongly correlated with-activation of ATM. This observation is consistent with the generally accepted paradigm that in most instances of DNA damage Chk2 phosphorylation is mediated by ATM.<sup>39-43</sup> The present data thus buttress this conclusion, and indicate that in the case of oxidative DNA damage, Chk2 also is the substrate of ATM. Moreover, the data shown in Figure 3 provide additional insight into the relationship between Chk2 activation and cell cycle arrest. Expression of Chk2-Thr68<sup>P</sup> when measured as an integrated value of IF increased early during the treatment with H<sub>2</sub>O<sub>2</sub>, predominantly in S-phase cells, and then *declined*. However in contrast to the integral, the maximal pixel representation of the activated Chk2, which stresses the punctate, highly condensed localization

of this kinase, actually *increased* with time of oxidant exposure (2 h and 4 h), specifically in G<sub>1</sub> phase cells. Most likely this is a reflection of the continuing arrest at the G<sub>1</sub> to S transition when Cdc25A is the Chk2 substrate. In contrast, the cells at the G<sub>1</sub> to S transition (Fig. 3, bottom right two panels) have both low Chk2-Thr68<sup>P</sup> integrated as well as maximal pixel values, similar to that of S-phase cells.

The observation that the level of Mre11 recruitment was similar in all phases of the cell cycle, whereas the events downstream of the DNA damage response (i.e., ATM and Chk2 activation and H2AX phosphorylation) were maximal in S phase cells is intriguing. This observation suggests that the recruitment of Mre11 after oxidative DNA damage, as measured immunocytochemically, was not as effective, per se, in activating ATM and subsequent events of the damage response in G<sub>1</sub> and G<sub>2</sub>M cells as it was in S-phase cells. The cell cycle-phase specific factors thus appear to modulate activation of the events subsequent to Mre11 recruitment.

We have recently described the activation of ATM and Chk2 and the phosphorylation of H2AX phosphorylation (as measured by cytometry) upon induction of DNA damage by DNA topoisomerase I and II inhibitors topotecan (TPT) or mitoxantrone (MXT), respectively.<sup>53</sup> The kinetics of phosphorylation of these proteins in response to DNA damage by the topoisomerase inhibitors was different than those observed here in cells treated with H<sub>2</sub>O<sub>2</sub>. Chk2 activation in cells treated either with TPT or MXT was much slower compared to the treatment with H<sub>2</sub>O<sub>2</sub>. Specifically, whereas the peak of activation was seen 4 h after administration of these inhibitors Chk2 activation peaked at 10 min in cells treated with H<sub>2</sub>O<sub>2</sub> (Figs. 2 and 5). Furthermore, the peak of H2AX phosphorylation, seen 2 h after treatment with TPT or MXT, preceded by 2 h the maximal level of Chk2 activation. In cells treated with H<sub>2</sub>O<sub>2</sub> the peaks of activation of Chk2 and phosphorylation were temporarily coincident. Clearly thus, different types of DNA damage such as caused by DNA topoisomerase inhibitors versus H<sub>2</sub>O<sub>2</sub> induce quite different kinetics of DNA damage response.

The punctate expression of activated Chk2 both in untreated and H<sub>2</sub>O<sub>2</sub> treated cells was underscored by cytometry when represented as maximal pixel rather than integrated value of immunofluorescence (IF) per nucleus and as discussed was most pronounced in G<sub>1</sub> cells, which likely reflects activation of the G<sub>1</sub> to S transition checkpoint by Chk2. In untreated cultures subpopulations of G<sub>1</sub> and G<sub>2</sub>M cells with strong maximal pixel of Chk2-Thr68<sup>P</sup> IF in relation to centrosomes were present. Cytometric multiparameter assessment of DNA damage response, particularly with the use of quantitative image analysis that allows one to measure the inhomogeneity of distribution (e.g., maximal pixel) of each fluorochrome, provides unique advantages in studies of the correlation in response of different cell constituents to the damage as a function of cell cycle position.

## Materials and Methods

### Cells, cell treatment

A549 cells, obtained from American Type Culture Collection (ATCC; Manassas, VA), were grown in Ham's F-12K Nutrient Mixture (Mediatech, Inc., Manassas, VA) supplemented with 10% fetal bovine serum, 100 units/ml penicillin, 100 µg/ml streptomycin and 2 mM L-glutamine (GIBCO/BRL; Grand Island, NY) in 25 ml FALCON flasks (Becton Dickinson Co., Franklin Lakes, NJ) at 37.5°C in an atmosphere of 95% air and 5% CO<sub>2</sub>. The cells were maintained in exponential and asynchronous phase of growth by repeated trypsinization and reseeding prior to reaching subconfluency. The cells were then trypsinized and seeded at low density (about 5 × 10<sup>4</sup> cells per chamber) in 2-chambered Falcon CultureSlides (Beckton Dickinson). Twenty four hours after seeding the cultures were treated with 200 µM H<sub>2</sub>O<sub>2</sub>

(Sigma Chemical Co., St. Louis, MO) for different time intervals, as described in the legends to figures. Control cultures were treated with the equivalent volumes of distilled water.

### Detection of Mre11, phosphorylation of ATM on Ser 1981, Chk2 phosphorylation on Thr 68 and H2AX phosphorylation on Ser 139

Following incubations with H<sub>2</sub>O<sub>2</sub> the cells were rinsed with PBS and then fixed with 1% methanol-free formaldehyde (Polysciences, Inc., Warrington, PA) in PBS for 15 min on ice followed by suspension in 70% ethanol where they were stored at -20°C for 2–24 h. The fixed cells were then washed twice in PBS and treated on slides with 0.1% Triton X-100 (Sigma) in PBS for 15 min, and then in a 1% (w/v) solution of bovine serum albumin (BSA; Sigma) in PBS for 30 min to suppress nonspecific antibody (Ab) binding. The cells were then incubated in 100 ml volume of 1% BSA containing 1:200 dilution of phospho-specific (*Ser-139*) histone H2AX ( $\gamma$ H2AX) mouse monoclonal antibody (mAb) (BioLegend, San Diego, CA), or 1:500 dilution of Mre11 (31H4) rabbit Ab, or a 1:100 dilution of phospho-specific ATM (*Ser-1981*) mAb (Upstate Cell Signaling, Temecula, CA), or 1:100 dilution of phospho-specific (*Thr-68*) Chk2 rabbit polyclonal antibody (Cell Signaling). After overnight incubation at 4°C, the slides were washed twice with PBS and then incubated in 100 ml of 1:100 dilution of Alexa Fluor 488 goat anti-mouse (H2AX) or anti-rabbit IgG (H + L) (Chk2 and Mre11), or 1:50 dilution of Alexa Fluor 633 goat anti-mouse (ATM) (all from Invitrogen /Molecular Probes, Eugene OR), respectively, for 45 min at room temperature in the dark. The cells were then counterstained with either 2.8  $\mu$ g/ml 4,6-diamidino-2-phenylindole (DAPI; Sigma) in PBS for 15 min (in samples to be analyzed by laser scanning cytometry (LSC),<sup>53,54</sup> or 5  $\mu$ g/ml of 7-aminoactinomycin D (7-AAD) (Invitrogen/Molecular Probes) in the samples to be analyzed by fluorescence microscopy.

### Measurement of cell fluorescence by LSC

Cellular green IF representing expression of  $\gamma$ H2AX, ATM-S1981<sup>P</sup>, Mre11 or of activated (Thr68 phosphorylated) Chk2 and blue emission of DAPI was measured by LSC (iCys; CompuCyte, Cambridge, MA) utilizing standard filter settings; fluorescence was excited with 488-nm argon ion and violet diode lasers, respectively.<sup>8,54</sup> The intensities of maximal pixel and integrated fluorescence were measured and recorded for each cell. At least 3,000 cells were measured per sample. Gating analysis was carried out to obtain mean values ( $\pm$ SE) of  $\gamma$ H2AX IF or Chk2Thr68<sup>P</sup> for G<sub>1</sub> (DNA Index; DI = 0.9–1.1), S (DI = 1.2–1.8) and G<sub>2</sub>M (DI = 1.9–2.1) cell populations in each experiment. To express the treatment-induced changes in IF (6; Fig. 5) the mean IF values for G<sub>1</sub>, S and G<sub>2</sub>M cell populations estimated for the untreated cells (Ctrl) were subtracted from the respective mean values of the cells treated with H<sub>2</sub>O<sub>2</sub>, for each time-point of the treatment. The SE was estimated based on Poisson distribution of cell populations. Each experiment was run at least in triplicate, some experiments were additionally repeated. The inter-sample variations were not statistically significant; the representative raw data in form of bivariate distributions (scatterplots) are shown in Figures 1–4. Other details were provided before<sup>8</sup> or are given in figure legends.

### Acknowledgements

Supported by NCI; Grant number CA 28704.

### References

1. Beckman BK, Ames BN. The free radical theory of aging matures. *Phys Rev* 1998;78:547–81.
2. Beckman KB, Ames BN. Oxidative decay of DNA. *J Biol Chem* 1997;272:13300–5.
3. Gorbunova V, Seluanov A. Making ends meet in old age: DSB repair and aging. *Mech Ageing Dev* 2005;126:621–8. [PubMed: 15888314]

4. Karanjawala ZE, Lieber MR. DNA damage and aging. *Mech Ageing Dev* 2004;125:405–16. [PubMed: 15272504]
5. Parrinello S, Samper E, Krtolica A, Goldstein J, Melov S, Campisi J. Oxygen sensitivity severely limits the replicative lifespan of murine fibroblasts. *Nat Cell Biol* 2003;5:741–7. [PubMed: 12855956]
6. Schriener SE, Linford NJ, Martin GM, Treuting P, Ogburn CE, Emond M, Coskun PE, Ladiges W, Wolf N, Van Remmen H, Wallace DC, Rabinovitch PS. Extension of murine life span by overexpression of catalase targeted to mitochondria. *Science* 2005;308:1875–8. [PubMed: 15976292]
7. Vilenchik MM, Knudson AG. Endogenous DNA double-strand breaks: Production, fidelity of repair, and induction of cancer. *Proc Natl Acad Sci USA* 2003;100:12871–6. [PubMed: 14566050]
8. Zhao H, Tanaka T, Halicka HD, Traganos F, Zarebski M, Dobrucki J, Darzynkiewicz Z. Cytometric assessment of DNA damage by exogenous and endogenous oxidants reports the aging-related processes. *Cytometry A* 2007;71:905–14. [PubMed: 17879239]
9. Tanaka T, Halicka HD, Huang X, Traganos F, Darzynkiewicz Z. Constitutive histone H2AX phosphorylation and ATM activation, the reporters of DNA damage by endogenous oxidants. *Cell Cycle* 2006;5:1940–5. [PubMed: 16940754]
10. Taioli E, Sram RJ, Garte BM, Kalina I, Popov TA, Farmer PB. Effects of polycyclic aromatic hydrocarbons (PAHs) in environmental pollution on exogenous and oxidative DNA damage (EXPAH project): description of the population under study. *Mutat Res* 2007;620:1–6. [PubMed: 17420032]
11. Tanaka T, Halicka HD, Traganos F, Darzynkiewicz Z. Phosphorylation of histone H2AX on Ser 139 and activation of ATM during oxidative burst in phorbol ester-treated human leukocytes. *Cell Cycle* 2006;5:2671–5. [PubMed: 17106266]
12. Shacter E, Beecham EJ, Covey JM, Kohn KW, Potter M. Activated neutrophils induce prolonged DNA damage in neighboring cells. *Carcinogenesis* 1988;9:2297–304. [PubMed: 2847879]
13. Chong YC, Heppner GH, Paul LA, Fulton AM. Macrophage-mediated induction of DNA strand breaks in target tumor cells. *Cancer Res* 1989;49:6652–7. [PubMed: 2819715]
14. Demirbag R, Yilmaz R, Kocyigit A, Guzel S. Effect of coronary angiography on oxidative DNA damage observed in circulating lymphocytes. *Angiology* 2007;58:141–7. [PubMed: 17495261]
15. Cadet J, Delatour T, Douki T, Gasparutto D, Pouget JP, Ravanat JL, Sauvaigo S. Hydroxyl radicals and DNA base damage. *Mutat Res* 1999;424:9–21. [PubMed: 10064846]
16. Marnett LJ. Oxy radicals, lipid peroxidation and DNA damage. *Toxicology* 2002;181:219–22. [PubMed: 12505314]
17. Pastwa E, Blasiak J. Non-homologous DNA end joining. *Acta Biochim Pol* 2003;50:891–908. [PubMed: 14739985]
18. Jeggo PA, Lobrich M. Artemis links ATM to double strand end rejoining. *Cell Cycle* 2005;4:359–62. [PubMed: 15684609]
19. Blagosklonny MV. Aging and immortality: Quasi-programmed senescence and its pharmacologic inhibition. *Cell Cycle* 2006;5:2087–102. [PubMed: 17012837]
20. Blagosklonny MV. Paradoxes of aging. *Cell Cycle* 2007;6:2997–3003. [PubMed: 18156807]
21. Mallette FA, Ferbeyre G. The DNA damage signaling pathway connects oncogenic stress to cellular senescence. *Cell Cycle* 2007;6:1831–6. [PubMed: 17671427]
22. Tanaka T, Kurose A, Halicka HD, Traganos F, Darzynkiewicz Z. 2-Deoxy-D-glucose reduces the level of constitutive activation of ATM and phosphorylation of histone H2AX. *Cell Cycle* 2006;5:878–82. [PubMed: 16628006]
23. Tanaka T, Kajstura M, Halicka HD, Traganos F, Darzynkiewicz Z. Constitutive histone H2AX phosphorylation and ATM activation are strongly amplified during mitogenic stimulation of lymphocytes. *Cell Prolif* 2007;40:1–13. [PubMed: 17227291]
24. Huang X, Tanaka T, Kurose A, Traganos F, Darzynkiewicz Z. Constitutive histone H2AX phosphorylation on Ser-139 in cells untreated by genotoxic agents is cell cycle phase specific and attenuated by scavenging reactive oxygen species. *Int J Oncol* 2006;29:495–501. [PubMed: 16820894]
25. Tanaka T, Halicka HD, Traganos F, Darzynkiewicz Z. Phosphorylation of histone H2AX on Ser 139 and activation of ATM during oxidative burst in phorbol ester-treated human leukocytes. *Cell Cycle* 2006;5:2671–5. [PubMed: 17106266]

26. Tanaka T, Kurose A, Halicka HD, Huang X, Traganos F, Darzynkiewicz Z. Nitrogen oxide-releasing aspirin induces histone H2AX phosphorylation, ATM activation and apoptosis preferentially in S-phase cells; involvement of reactive oxygen species. *Cell Cycle* 2006;5:1669–74. [PubMed: 16861926]
27. Sedelnikova OA, Rogakou EP, Panuytin IG, Bonner W. Quantitative detection of <sup>125</sup>IUdr-induced DNA double-strand breaks with  $\gamma$ -H2AX antibody. *Radiation Res* 2002;158:486–92.
28. Lavin MF, Kozlov S. ATM activation and DNA damage response. *Cell Cycle* 2007;6:931–42. [PubMed: 17457059]
29. Bartkova J, Bakkenist CJ, Rajpert-De Meyts E, Skakkebaek NE, Sehested M, Lukas J, Kastan MB, Bartek J. ATM activation in normal human tissues and testicular cancer. *Cell Cycle* 2005;4:838–45. [PubMed: 15846060]
30. Olive PL. Detection of DNA damage in individual cells by analysis of histone H2AX phosphorylation. *Methods Cell Biol* 2004;75:355–73. [PubMed: 15603433]
31. Huang X, Okafuji M, Traganos F, Luther E, Holden E, Darzynkiewicz Z. Assessment of histone H2AX phosphorylation induced by DNA topoisomerase I and II inhibitors topotecan and mitoxantrone and by DNA crosslinking agent cisplatin. *Cytometry* 2004;58:99–110. [PubMed: 15057963]
32. Halicka HD, Huang X, Traganos F, King MA, Dai W, Darzynkiewicz Z. Histone H2AX phosphorylation after cell irradiation with UV-B: Relationship to cell cycle phase and induction of apoptosis. *Cell Cycle* 2005;4:339–45. [PubMed: 15655354]
33. Tanaka T, Kurose A, Huang X, Dai W, Darzynkiewicz Z. ATM kinase activation and histone H2AX phosphorylation as indicators of DNA damage by DNA topoisomerase I inhibitor topotecan and during apoptosis. *Cell Prolif* 2006;39:49–60. [PubMed: 16426422]
34. Kurose A, Tanaka T, Huang X, Traganos F, Dai W, Darzynkiewicz Z. Effects of hydroxyurea and aphidicolin on phosphorylation of ATM on Ser 1981 and histone H2AX on Ser 139 in relation to cell cycle phase and induction of apoptosis. *Cytometry A* 2006;69:212–21. [PubMed: 16528719]
35. Marti TM, Hefner E, Feeney L, Natale V, Cleaver JE. H2AX phosphorylation within the G<sub>1</sub> phase after UV irradiation depends on nucleotide excision repair and not DNA double-strand breaks. *Proc Natl Acad Sci USA* 2006;103:9891–6. [PubMed: 16788066]
36. Kataoka Y, Bindokas VP, Duggan RC, Murley JS, Grdina DJ. Flow cytometric analysis of phosphorylated histone H2AX following exposure to ionizing radiation in human microvascular endothelial cells. *J Radiat Res* 2006;47:245–57. [PubMed: 16960336]
37. Huang X, Halicka HD, Traganos F, Tanaka T, Kurose A, Darzynkiewicz Z. Cytometric assessment of DNA damage in relation to cell cycle phase and apoptosis. *Cell Prolif* 2005;38:223–43. [PubMed: 16098182]
38. Tanaka T, Huang X, Halicka HD, Zhao H, Traganos F, Albino AP, Dai W, Darzynkiewicz Z. Cytometry of ATM activation and histone H2AX phosphorylation to estimate extent of DNA damage induced by exogenous agents. *Cytometry A* 2007;71:648–61. [PubMed: 17622968]
39. Matsuoka S, Huang M, Elledge SJ. Linkage of ATM to cell cycle regulation by the Chk2 protein kinase. *Science* 1998;282:1893–7. [PubMed: 9836640]
40. Zhou BB, Elledge SJ. The DNA response: putting checkpoints in perspective. *Nature* 2000;408:433–9. [PubMed: 11100718]
41. Ahn J, Urist M, Prives C. The Chk2 protein kinase. *DNA repair* 2004;3:1039–47. [PubMed: 15279791]
42. Ahn JY, Schwartz JK, Piwnicka-Worms H, Canman CE. Threonine 68 phosphorylation by ataxia telangiectasia mutated is required for efficient activation of Chk2 in response to ionizing radiation. *Cancer Res* 2000;60:5934–6. [PubMed: 11085506]
43. Peng CY, Graves PR, Thoma RS, Wu Z, Shaw AS, Piwnicka-Worms H. Mitotic and G<sub>2</sub> checkpoint control.: regulation of 14-3-3 protein binding by phosphorylation of Cdc25C on serine-216. *Science* 1997;277:1501–5. [PubMed: 9278512]
44. Rudolph J. Cdc25 phosphatases: Structure, specificity and mechanism. *Biochemistry* 2007;46:3595–604. [PubMed: 17328562]
45. Boutros R, Dozier C, Ducommun B. The when and wheres of CDC25 phosphatases. *Curr Opin Cell Biol* 2006;18:185–91. [PubMed: 16488126]

46. Ray D, Kiyokawa H. CDC25 levels determine the balance of proliferation and checkpoint response. *Cell Cycle* 2007;6:3039–42. [PubMed: 18073536]
47. Lee JH, Paull TT. ATM activation by DNA double-strand breaks through the Mre11- Rad50-Nbs1 complex. *Science* 2005;308:551–4. [PubMed: 15790808]
48. Paull TT, Lee JH. The Mre11/Rad50/Nbs1 complex and its role as a DNA-double strand break sensor for ATM. *Cell Cycle* 2005;4:737–40. [PubMed: 15908798]
49. Abraham RT, Tibbetts RS. Guiding ATM to broken DNA. *Science* 2005;308:510–11. [PubMed: 15845843]
50. Downs JA, Cote J. Dynamics of chromatin during the repair of DNA double-strand breaks. *Cell Cycle* 2005;4:1373–6. [PubMed: 16205111]
51. Lavin MF. ATM and the Mre11 complex combine to recognize and signal DNA double-strand breaks. *Oncogene* 2007;26:7749–58. [PubMed: 18066087]
52. US patent No. 5,675,063.
53. Zhao H, Traganos F, Darzynkiewicz Z. Kinetics of histone H2AX phosphorylation and Chk2 activation in A549 cells treated with topotecan and mitoxantrone in relation to the cell cycle phase. *Cytometry A* 73A:480–9.
54. Darzynkiewicz Z, Bedner E, Gorczyca W, Melamed MR. Laser scanning cytometry. A new instrumentation with many applications. *Exp Cell Res* 1999;249:1–12. [PubMed: 10328948]

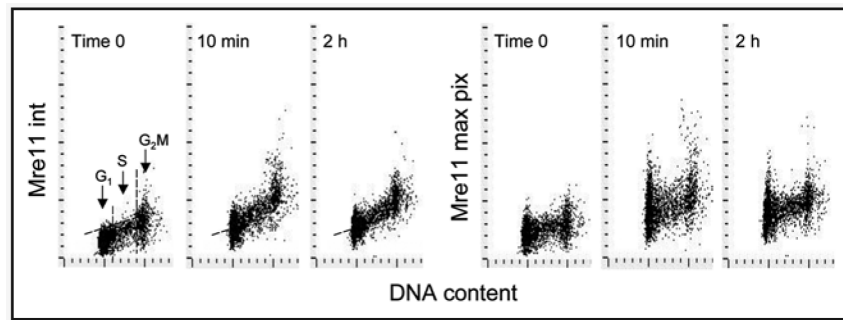


**Figure 1.**

Effect of exposure of A549 cells to  $H_2O_2$  on Mre11 expression. Exponentially growing A549 cells were left untreated (time 0) or were treated with  $200 \mu M H_2O_2$  for 10 min or 2 h then fixed and expression of Mre11 was measured by LSC within cell nuclei in conjunction with cellular DNA content. Bivariate distributions (DNA content vs Mre11 IF) showing expression of Mre11 either as integrated IF over the nucleus (int) or as maximal pixel IF (max pix), with respect to the cell cycle phase. The dashed skewed lines show the upper threshold level of Mre11 IF for 97% of interphase ( $G_1 + S$ ) cells in the untreated (time 0) culture. Maximal increase in Mre11 IF was observed during the initial 10 min and a decline was observed subsequently (see Fig. 5 for the kinetics data).

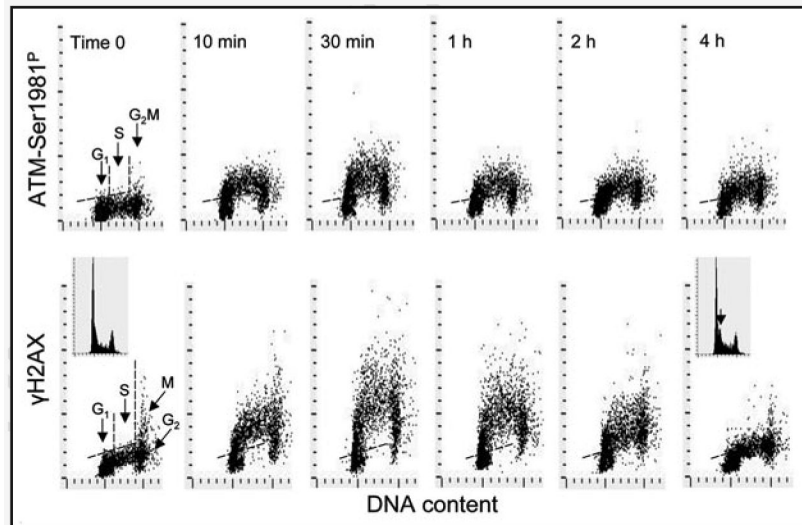


**Figure 2.**

Activation of ATM and phosphorylation of histone H2AX in A549 cells treated with H<sub>2</sub>O<sub>2</sub>. The cells were untreated (time 0) or treated in cultures with 200 μM H<sub>2</sub>O<sub>2</sub> for time periods as shown in the respective panels. Bivariate distributions (DNA content vs ATM-S1981<sup>P</sup>, or vs γH2AX IF) represent the IF of these phospho-proteins integrated over the nucleus with respect to cell cycle phase. The dashed skewed lines show the upper threshold level of ATM-S1981<sup>P</sup> or γH2AX IF for 97% of interphase (G<sub>1</sub> + S) cells in the untreated (time 0) cultures. The DNA content histograms in the bottom panels show the cell cycle distribution at time 0 and after 4 h of treatment with H<sub>2</sub>O<sub>2</sub>. A minor accumulation of very early S-phase cells is apparent after 4 h of treatment with H<sub>2</sub>O<sub>2</sub> (arrow).

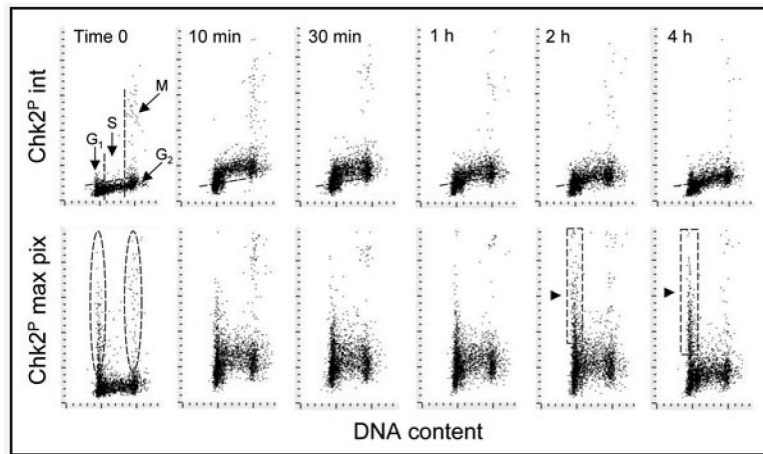


**Figure 3.**

Activation of Chk2 in A549 cells treated with  $H_2O_2$ . The cells were untreated (time 0) or treated in cultures with  $200 \mu M H_2O_2$  for the length of time shown in the respective panels. Bivariate distributions (DNA content vs Chk2Thr68<sup>P</sup> IF) showing expression of Chk2Thr68<sup>P</sup> either as integrated IF over the nucleus (int) or as maximal pixel IF (max pix), with respect to cell cycle phase. As in Figures 1 and 2, the skewed dashed lines represent the upper threshold level of Chk2-Thr68<sup>P</sup> IF for 97% of interphase ( $G_1 + S$ ) cells in the untreated (time 0) cultures. See the text describing cell subpopulations marked by dashed boundaries.

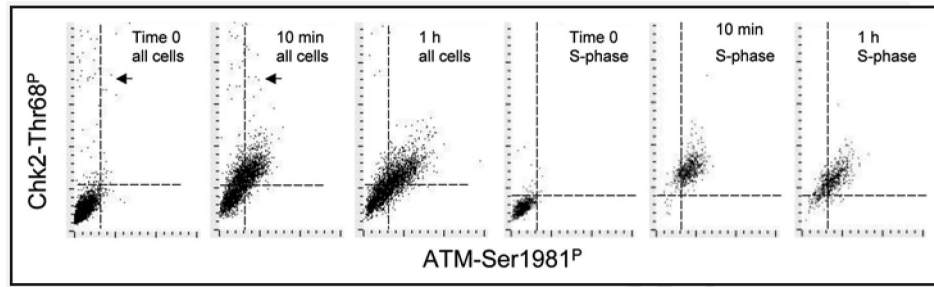


**Figure 4.**

Correlation between activation of ATM and Chk2 during A549 cells in response to oxidative stress. Bivariate (ATM-S1981<sup>P</sup> vs Chk2-Thr68<sup>P</sup> IF) distributions of cells treated with 200  $\mu$ M H<sub>2</sub>O<sub>2</sub> for 10 min or 1 h. (A–C) show all cells, (D–F) show S-phase cells gated based on differences in DNA content as described in Materials and Methods. The dashed horizontal or vertical lines show the upper thresholds values of Chk2-Thr68<sup>P</sup> IF or ATM-Ser1981<sup>P</sup> IF for 97% cells from the untreated (time 0) culture, respectively.

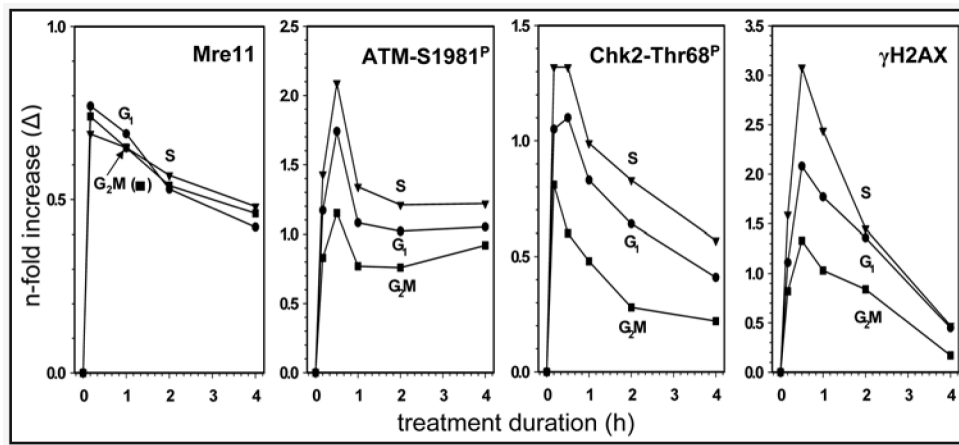


**Figure 5.** Kinetics of Mre11 recruitment, ATM and Chk2 activation, and H2AX phosphorylation in A549 cells exposed to 200  $\mu$ M H<sub>2</sub>O<sub>2</sub> for different time intervals. The means values of Mre11, ATM-S1981<sup>P</sup>, Chk2-Thr68<sup>P</sup> and  $\gamma$ H2AX IF were estimated for subpopulations of cells in G<sub>1</sub>, S and G<sub>2</sub>M, untreated (time 0) and treated with H<sub>2</sub>O<sub>2</sub>, by gating analysis based on differences in DNA content, as described in Materials and Methods. The respective mean values of the untreated cells were subtracted from the means of the treated ones and the H<sub>2</sub>O<sub>2</sub>-induced change ( $\Delta$ ) was plotted as n-fold increase over the respective mean values of the untreated cells.

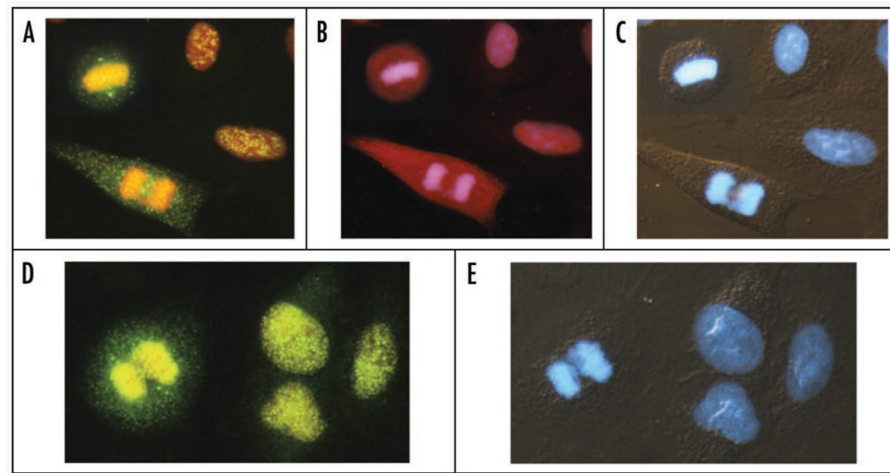


**Figure 6.**

Expression of Chk2-Thr68<sup>P</sup>, ATM-S1981<sup>P</sup> and Mre11 in A549 cells treated with 200  $\mu$ M H<sub>2</sub>O<sub>2</sub> for 10 min. Expression of Chk2-Thr68<sup>P</sup> (A) and ATM-S1981<sup>P</sup> (B) in two interphase and two mitotic cells. The metaphase cell within the inset is from another field of view, shown to demonstrate localization of activated Chk2 in centrosomes. (D) shows expression of Mre11, also with its distinct presence in centrosomes. The cells were immunocytochemically stained with Alexa Fluor 488 (A and D) or Alexa Fluor 633 (B) and their DNA was counterstained concurrently with 7-AAD (A, B and D) and DAPI (C and E). Cells shown in (C and E) were viewed under combined UV epifluorescence and Nomarski interference contrast illumination.